A Monte Carlo simulation study of the impact of novel scintillation crystals on performance characteristics of PET scanners

Amir Ghabrial[a,b], Daniel Franklin[b], Habib Zaidi[a]

[a]*Division of Nuclear Medicine and Molecular Imaging, Geneva University Hospital, CH-1211 Geneva, Switzerland*
[b]*University of Technology Sydney, Ultimo NSW 2007, Sydney Australia*

Abstract

Objective: The purpose of this study is to validate a Monte Carlo simulation model for the clinical Siemens Biograph mCT PET scanner using the GATE simulation toolkit, and to evaluate the performance of six different scintillation materials in this model using the National Electrical Manufactures Association (NEMA) NU 2-2007 protocol.

Methods: A model of the Biograph mCT PET detection system and its geometry was developed. NEMA NU 2-2007 phantoms were also modelled. The accuracy of the developed scanner model was validated through a comparison of the simulation results from GATE, SimSET and PeneloPET toolkits, and experimental data obtained using the NEMA NU 2-2007 protocols. The evaluated performance metrics included count rate performance, spatial resolution, sensitivity, and scatter fraction (SF). Thereafter, the mCT PET scanner was simulated with six different candidate high-performance scintillation materials, including LSO, $LaBr_3$, $CeBr_3$, LuAP, GLuGAG and LFS-3, and its performance evaluated according to the NEMA NU 2-2007 specifications.

Results: The Monte Carlo simulation model demonstrates good agreement with the experimental data and results from other simulation packages. For instance, the scatter fraction calculated using GATE simulation is 34.35% while the experimentally measured value is 33.2%, 38.48% for the SimSET, and 34.8% for the PeneloPET toolkit. The best-performing scintillation materials were found to be LuAP, LSO and LFS-3, while GLuGAG offers acceptable performance if cost is the dominant concern.

Conclusion: The main performance characteristics of the Biograph mCT PET scanner can be simulated accurately using GATE with a good agreement with other Monte Carlo simulation packages and experimental measurements.

☆Corresponding Author: Habib Zaidi, Ph.D, Geneva University Hospital, Division of Nuclear Medicine and Molecular Imaging, CH-1211 Geneva, Switzerland, Tel: +41 22 372 7258; Fax: +41 22 372 7169.

Email address: habib.zaidi@hcuge.ch (Habib Zaidi)

Newly developed scintillators show promise and offer alternative options for the design of novel generation PET scanners.

---

1. Introduction

Positron Emission Tomography (PET) is a well-established non-invasive molecular imaging modality enabling the in vivo assessment of molecular targets for a wide range of diseases. Recently, there have been a number of significant technological advances in PET scanners design, such as the development of new scintillation materials, novel image reconstruction algorithms, hybrid systems, such as PET-CT and PET-MRI, time-of-flight PET, dynamic (4D) PET imaging and whole-body parametric imaging, that collectively improve image quality and quantitative accuracy and broaden the range of clinical applications for which PET may be used.

Monte Carlo simulation methods are widely used for evaluating nuclear medical imaging systems owing to the stochastic nature of radiation emission and detection [1]. The OpenGATE collaboration developed a simulation tool, *Geant4 Application for Tomographic Emission (GATE)*, for modelling tomographic imaging systems such as, PET, SPECT and CT [2]. GATE provides a convenient platform enabling to quickly develop a realistic model of a tomographic scanner using the Geant4 (GEometry ANd Tracking) Monte Carlo simulation framework, without the need to write C++ code [3, 4]. GATE includes accurate models for the detector response (including optional optical photon tracking within an individual scintillation crystal), radiation emission via radioactive decay (with several models available, trading accuracy for speed), and moving source and/or detector components [2, 5]. In this work, we concentrate on the simulation of PET scanners.

GATE enables acucurate simulation of PET scanners, including relevant models for scintillator material properties, detector electronics and complex phantom/source geometries [5]. A number of validation studies for diverse PET scanners have previously been published, such as the GE Advance/Discovery LS [6], the Siemens Biograph^{TM}6 [7] and the Philips Allegro/Gemini scanners [8]. Several other PET simulation frameworks have also been used to validate the Siemens Biograph mCT PET scanner, including SimSET [9] and PeneloPET simulation toolkits [10]. Similar studies for evaluating different scintillation materials were also reported [11, 12, 13].

The purpose of this study is to perform a quantitative comparison of a number of promising new candidate scintillator materials for PET systems, using an accurate model of the Siemens Biograph mCT PET/CT system (Siemens Healthcare, Erlangen) as a reference scanner. A model of this scanner has been implemented in GATE, which has been fully characterised with LSO scintillators (as per the original scanner design) in terms of sensitivity, noise equivalent

count rate and scatter fraction in accordance with the NEMA NU 2-2007 protocol [14, 15, 16]. The results are compared with previously reported experimental results and simulation studies performed with other simulation platforms, to establish the validity of the GATE model. The same model is then built with five alternative scintillator materials, and the same scanner characteristics are evaluated according to the NEMA NU 2-2007 protocol. The performance evaluation aims to determine which of these new materials will offer the best performance for a low-cost PET scanner suitable for clinical and research applications.

2. Materials and Methods

2.1. The Biograph mCT PET scanner geometry

The scanner's detector array consists of 32,448 4 mm × 4 mm × 20 mm LSO crystals, structured in 4 rings of 48 detector blocks each, with a ring diameter of 84.2 cm. Each block comprises a 13×13 matrix of individual crystals, and each block is coupled to 4 photomultiplier tubes (PMTs). Therefore, each ring contains 8112 (13×13×48) crystals. The axial field of view (FOV) covers 218 mm, corresponding to 109 image planes with a slice thickness of 2 mm (three gaps of 4 mm between block rings are considered virtual rings; the total number of direct detection planes is thus 52+3 and the total number of indirect-detection planes is 51+3, for a total of 109). Data are acquired with a maximum ring difference of 49. The energy acceptance window is 435 keV to 650 keV, and the coincidence time window is 4.1 ns [17].

The NEMA performance tests are the standard benchmark used for performance evaluation of PET systems and to compare performance between different PET systems. In this work, the NEMA NU 2-2007 standards are used to evaluate, and validate the developed Siemens mCT PET scanner GATE model [14]. Although newer versions of this standard have been published, measured performance parameters have been provided using the 2007 standard [17]; therefore, this standard is used throughout this work.

The key system performance characteristics including sensitivity, scatter fraction, and spatial resolution have been evaluated according to the NEMA NU 2-2007 specifications [14]. The system model simulated in GATE is shown in Figure 1 whereas the scanner design parameters are listed in Table 1.

2.2. Monte Carlo simulation model validation

Validation of a GATE model for the mCT PET scanner is essential to perform meaningful predictive simulation studies for evaluating the performance of different candidate scintillation materials for high performance PET scanners. The NEMA NU 2-2007 standard tests for the sensitivity, scatter fraction, and spatial resolution parameters have been developed using GATE and ROOT [18], with the purpose of providing a complete description of the mCT PET scanner performance in whole body imaging.

2.2.1. Spatial resolution

The NEMA NU 2-2007 spatial resolution evaluation protocol was applied to determine the point spread function (PSF) of the scanner at different points inside the field-of-view. The spatial resolution is expressed in terms of full width at half-maximum (FWHM) and full width at tenth-maximum (FWTM) of the reconstructed image of a compact radioactive point source, measured across the radial, tangential and axial profiles through the peak of the activity distribution using the AMIDE 3D/4D image viewer [19]. For each profile, the width of the response functions in the other two dimensions is set to twice the FWHM, and the FWHM (and FWTM) is determined by linearly interpolating between adjacent pixels at half (or one tenth) of the maximum response function value.

A simulated source/phantom was constructed in GATE, consisting of a hollow glass capillary, 700 mm in length, parallel to the axis of the scanner, with an inner diameter of 1 mm and outer diameter of 2 mm. The source activity is contained within a 1 mm diameter sphere at the centre of the capilliary containing 3.9 MBq of ^{18}F. The source/phantom are translated to six positions within the scanner's FOV as illustrated in Figure 2: three in the transaxial plane passing through the centre of the scanner, at locations $(x, y, z) = (0, 10, 0)$ mm, $(0, 100, 0)$ mm and $(100, 0, 0)$ mm, and three in corresponding locations in the transaxial plane at one-quarter of the length of the axial field-of-view ($z = 54.5$ mm), i.e. $(x, y, z) = (0, 10, 54.5)$ mm, $(0, 100, 54.5)$ mm and $(100, 0, 54.5)$ mm.

Raw list-mode data are acquired for a simulated period of 20 minutes. The sinograms for each of the six points were then normalised, arc-corrected and single slice rebinned (SSRB) and converted to units of counts per second using STIR without any smoothing filters applied [20]. Each rebinned sinogram is then reconstructed into a matrix using two-dimensional (2D) filtered backprojection (FBP2D) implemented in STIR [20] and stacked to produce a $400 \times 400 \times 109$ volume, with voxel dimensions of $2.04\ mm \times 2.04\ mm \times 2.027\ mm$. The full-width at half maximum (FWHM) and full-width at tenth maximum (FWTM) of the reconstructed point source were measured in each dimension using linear interpolation.

2.2.2. Scatter fraction (SF) and count rate performance

The scatter fraction (SF) is evaluated according to the NEMA NU 2-2007 standard, using a NEMA scatter phantom. The NEMA scatter phantom is a polyethylene cylinder of density $\rho = 0.96$ g/cm^3 with an outside diameter of 200 mm and length of 700 mm, with an off-axis cylindrical hole of diameter 6.4 mm located at a radial distance of 45 mm, parallel to the central axis of the phantom cylinder. A simulated line source is placed within an 800 mm hollow polyethylene tube with an inside diameter of 3.2 mm and an outside diameter of 4.8 mm. The line source tube is placed within the hole in the phantom and filled with ^{18}F solution with activity concentrations of up to 45 kBq/ml.

The scatter fraction (SF) is estimated using the simulated events direct binning Eq. (1):

$$SF = \frac{C_S}{C_S + C_T} \tag{1}$$

where C_S is the number of scattered coincidences and C_T is the number of the true coincidences. The scatter fraction calculation is determined by direct binning of the simulated coincidence events instead of proceeding through the NEMA analysis, as the difference between the SF direct binning and the NEMA analysis is within 1% for a high count of true coincidence events [6].

The noise equivalent count rate (NECR) is calculated using Eq. (2).

$$NECR = \frac{C_T^2}{C_S + C_T + \kappa C_R} \tag{2}$$

where C_R is the number of random coincidences. The value of κ should be 1 for the case of direct NECR measurements, where the calculation of the singles rate represents a noiseless random correction, and 2 if the method of delayed subtraction is used [14].

2.2.3. Sensitivity

The NEMA NU 2-2007 sensitivity phantom consists of a 700 mm line source surrounded by up to five concentric 700 mm aluminium tubes, with inner/outer diameters of 3.9/6.4, 7.0/9.5, 10.2/12.7, 13.4/15.9 and 16.6/19.1 mm, respectively, which may be placed around the line source [14].

The simulated line source is a hollow polyethylene tube with an inner diameter of 1 mm and outer diameter of 3 mm, uniformly filled with 3.9 MBq of ^{18}F solution. The activity concentration was chosen to ensure that single event counting losses are below 1% and the rate of randoms is less than 5% of the true coincidence event rate [10].

The line source is placed at the desired location within the scanner, initially surrounded by the first aluminium tube only. Attenuation is progressively increased by adding successive aluminium tubes around the source. The simulation runs until a minimum of 10000 true coincidences per slice are collected.

The sensitivity is evaluated at two radial locations - one at the centre of the transaxial field-of-view, and one at a 100 mm radial offset. For each radial position, five simulations were performed (with the placement of 1-5 cylinders, respectively).

2.3. Potential inorganic scintillation materials

The performance of a PET scanner can be improved by increasing the sensitivity, extending the axial FOV (which also increases sensitivity), reducing random rates and scatter fraction, improving maximum count rate, minimising dead time, and improving spatial resolution. In particular, the scintillation material type, scintillation crystal dimensions and detector geometry have a large influence on PET scanner performance. Classical PET scanners typically use inorganic scintillator materials, such as cerium-doped Lutetium Oxyorthosilicate (Lu_2SiO_5) (LSO) or Cerium-doped Lutetium Yttrium Orthosilicate

($Lu_{1.8}Y_{0}.2SiO_{5}$) (LYSO), since these offer a combination of high density and effective atomic number, low optical attenuation at the peak scintillation output wavelength, high efficiency and fast decay time, making them well-suited for PET applications. However, in the past two decades, a number of new inorganic scintillator materials have emerged as potential candidates for PET.

The GATE model of the Biograph mCT PET scanner was modified by replacing its LSO scintillators by a number of promising candidate scintillator materials, which share the properties of fast response time and high light output, but with varying stopping power, output wavelength and effective atomic number: $LaBr_3$, $CeBr_3$, LuAP, GLuGAG and LFS-3. The other scanner parameters, including geometry, detection system and crystal size, remain unchanged. As such, optimization of crystal length according to crystal properties to achieve optimal performance was not considered. The performance characteristics of the PET scanner were evaluted with each of the proposed scintillator materials according to the NEMA NU-2 2007 protocol, including sensitivity, noise equivalent count rate and scatter fraction [14].

The properties of each of the selected candidate materials is described in the following subsections.

2.3.1. LSO

Cerium-doped lutetium oxyorthosilicate (Lu_2SiO_5:Ce) is an established PET scintillator [21] with an effective atomic number (Z_{eff}) of 66, high density (ρ) of 7.4 g/cm^3, refractive index n of 1.82, and a radiation attenuation length of 1.14-1.23 cm at 511 keV. The decay time is approximately 40 ns, the light output is approximately 22000-38800 photons/MeV (depending on dopant concentration) with a peak emission wavelength of 420 nm, and the obtainable energy resolution is 7.7-8.4% FWHM at 511 keV, with a photoelectric fraction of 32% [22, 23, 24, 25]. LSO offers a significant advantage over several other high-performance scintillators, being not hygroscopic.[26]

2.3.2. LaBr₃

Cerium-doped lanthanum bromide ($LaBr_3$:Ce) is a tri-halide scintillation material offering very high scintillation light output, fast decay time and good energy resolution. Its effective atomic number of 46 and density of 5.08 g/cm^3 are both lower than LSO, while its refractive index is similar at 1.90. Its radiation attenuation length at 511 keV is 2.13 cm [24, 27]. The decay time is approximately 16-30 ns (depending on dopant concentration), light output is approximately 63000 photons/MeV with a peak emission wavelength of 358-380 nm (both also depending on dopant concentration), and energy resolution is approximately 2.6% FWHM at 511 keV [28]. The photoelectric fraction is approximately 13%. $LaBr_3$:Ce is hygroscopic, even more so than NaI(Tl) [29].

2.3.3. CeBr₃

Cerium bromide ($CeBr_3$) is another tri-halide scintillation material which, like $LaBr_3$:Ce offers high scintillation light output, albeit with the drawback of hygroscopicity. Its physical and optical properties are quite similar to $LaBr_3$:

effective atomic number is 45.9, density is 5.10 g/cm^3 and refractive index is 2.09. Its radiation attenuation length at 511 keV is 2.10 cm [30]. The decay time is approximately 19 ns (depending on dopant concentration), light output is approximately 60000 photons/MeV with a peak emission wavelength of 371-380 nm (both also depending on dopant concentration), and energy resolution is approximately 3.6-3.8% FWHM at 511 keV [31].

2.3.4. LuAP

Cerium-doped Lutetium aluminium perovskite (LuAlO$_3$:Ce) is a fast, high-density scintillation material. Its effective atomic number is 65, density is 8.34 g/cm^3 and refractive index is 1.94. Its radiation attenuation length at 511 keV is 1.10 cm. The decay time is approximately 17 ns (depending on dopant concentration), light output is approximately 11400 photons/MeV with a peak emission wavelength of 365 nm (both also depending on dopant concentration) [32], the obtainable energy resolution is approximately 9% FWHM at 511 keV with a photoelectric fraction of 32%. LuAP is not hygroscopic and shares many properties of LSO, but with higher density and lower optical photon yield [33]. However, as yet LuAP has found limited application in PET, since producing large quantities of perovskite crystals with uniform properties has proven to be challenging [34].

2.3.5. GLuGAG

((Gd$_x$Lu$_{1-x}$)$_3$(Ga$_y$Al$_{1-y}$)$_5$O$_{12}$:Ce) is a cerium-doped lanthanide gallium aluminium rare-earth ceramic garnet (polycrystalline) scintillation material, whose physical properties vary significantly depending on the specifics of its manufacture, and the addition of co-dopants [35]. It is related to other ceramic garnet scintillator materials such as GAGG:Ce, with some fraction of the gadolinium replaced with lutetium [36]. Its effective atomic number is 55.2, density is 6.7-7.1 g/cm^3 and refractive index is 1.92. Its radiation attenuation length at 511 keV is 1.3-1.5 cm. Scintillation time constants of approximately 50 ns and 84/148 ns (fast/slow) have been reported in the literature [37]; light output is reported to be between 48200 and 60000 photons/MeV with a peak emission wavelength of 540 nm. The obtainable energy resolution is approximately 7.1% FWHM at 662 keV, and the scintillator is not hygroscopic [38].

2.3.6. LFS-3

Lutetium Fine Silicate (LFS-3) is a recently-introduced co-doped (with dopants including Ce, Gd, Sc, Y, La, Tb, and Ca) scintillator material related to LSO. LFS-3 has an effective atomic number of 64, density is 7.35 g/cm^3 and refractive index is 1.81 [39]. Its radiation attenuation length at 511 keV is 1.15 cm. The decay time is approximately 33-36 ns (depending on dopant concentration), light output is approximately 20000-35500 photons/MeV with a peak emission wavelength of 425-435 nm (both also depending on dopant concentration), The obtainable energy resolution is approximately 8% FWHM at 511 keV [40]. The scintillator is not hygroscopic.

2.4. Specific material parameters

As most of the scintillator materials discussed in the preceding section have been observed to exhibit a range of physical properties, it is necessary to choose a set of parameters for each material to use in the simulation study. The full list of specific material parameters adopted in this work are presented in Table 2.

3. Results

The performance characteristics of the simulated PET scanner, comprising the spatial resolution, sensitivity, and scatter fraction, are summarised in Tables 3 and 4, respectively. A dead time of 80 ns was assumed for singles [41]. Through applying the filtered back-projection reconstruction algorithm, the characteristics of the spatial resolution were similar to the experimental mCT PET scanner results. The spatial resolution resulting sinograms for six points are illustrated in figure 2.

Scatter fractions of 34.35% were obtained, compared to previously published experimental values of 33.2%. This result is similar to that obtained from PeneloPET and closer to the experimental value than that obtained with SimSet. The NECR was found to be 188 kcps at an activity concentration of 25 kBq/mL, which is similar to the results obtained with SimSet but better than PeneloPET. The NECR curve is illustrated in Figure 4. The simulated count rate performance is illustrated in Figure 3.

The sensitivity was found to be 9.65 kcps/MBq, which is very close to the published experimental value of 9.7 kcps/MBq. The results for the two radial and axial positions (at CFoV and 100 mm) are shown in Figure 5.

The performance characteristics of the simulated mCT PET scanner using each of the potential scintillation material candidates are summarised in Table 5 and Figure 6.

4. Discussion

This work aims were to develop a MC model of the Siemens Biograph mCT PET scanner using the GATE simulation tool and validate its accuracy against experimental measurements. Thereafter, the same scanner was simulated using six different potential candidate scintillation materials: LSO, $LaBr_3$, $CeBr_3$, LuAP, GLuGAG and LFS-3, and its performance evaluated according to the NEMA NU 2-2007 specifications, including sensitivity, noise equivalent count rate (NECR) and scatter fraction (SF).

One of the limitations in this study was the excessive computation burden of GATE compared to other Monte Carlo simulation tools, as reflected by the time required per event from positron decay to coincident detection of annilation photons. However, a multi-threaded GATE execution on a cluster of computers with numerous nodes each with a varying number of cores, each core having 3.5GHz Intel Xeon E5-2643 v2, 25MB L3 Cache (Max turbo 3.8GHz), and 16GB

1600MHz ECC DDR3-RAM (Quad Channel) enabled to speed-up the execution by at least one order of magnitude compared to single-threaded simulations on the same cluster.

The simulated performance parameters obtained using a GATE model of the mCT PET scanner's geometry and detection system evaluated using the NEMA NU 2-2007 protocol, were in good agreement with published experimental results for the key performance metrics of spatial resolution, sensitivity, scatter fraction and noise equivalent count rate. Therefore, the modelled PET scanner geometry and detection system are valid and accurately reproduce the physical scanner as illustrated in Tables 3, 4.

However, few discrepancies were reported for some performance parameters between the experimental results obtained from the actual scanner and the GATE simulation model, which is probably due to the inefficiency in simulating the whole mCT PET scanner gemoetry and design configuration such as, optical coupling efficiencies between the PMTs and the block detectors, the patient bed (modelled as 2 cm thick plastic), optical transport, and attenuating material within the scanner gantry. The light sharing was not modelled for the block detectors, which eventually led to overestimation to the spatial resolution. Schmidtlein et al. [6], considered the crosstalk between the scintillation crystals by adding to the events position, a static Gaussian spatial blurring, to match the simulated and the experimental results. On the other hand, inhomogeneous axial blurring taking place due to the Gaussian blurring does not accurately model the events mis-positioning across a block detector, as the spatial blurring is dependent on the edge effects and the position.

The second aim, consequently, is to categorize a scintillator with the appropriate characteristics to match the requirements of the high performance optimal PET scan system. The optimal scintillation material should have high light yield to meet the required positioning accuracy, good energy resolution, high density (ρ) for high stopping power and photofraction for good sensitivity, and fast decay time (τ) to guarantee superb coincidence timing and low dead time. Candidates also should produce scintillation photons at a wavelength which is compatible with the spectral range of maximum sensitivity for the chosen photo detector technology (e.g. photomultiplier tubes, silicon photomultipliers or avalanche photodiode arrays) for maximum detection efficiency. If a higher fraction of annihilation photons can be captured, particularly as photoelectric interactions falling within the energy window of the detector, and the number of resulting scintillation photons accurately quantified, the probability that both annihilation photons are detected also increases. Therefore, for a given quantity of radiotracer, the signal to noise ratio can be maximised. For accurate coincidence detection, the time constant of the scintillator should also be short.

The GATE model of the Siemens Biograph mCT PET for different scintillation materials were investigated according to the NEMA NU 2-2007 specifications using the same dimensions for all the scintillation materials. This obviously doesn't correspond to the optimal configuration for most of them due to the different characteristics of each scintillation material.

Of the materials evaluated, LuAP appears to offer the best combination of

properties. The sensitivity is the highest of all the materials evaluated while the corresponding scatter fraction is amongst the lowest. LuAP's NECR is also the highest of all the materials up to an activity concentration of approximately 25kBq/mL, matching the performance of LSO beyond this threshold. However, LuAP is challenging to manufacture and would currently be one of the most expensive materials to employ. The GLuGAG rare earth ceramic garnet offers a combination of good scintillation characteristics with high transparency and relatively low-cost fabrication. Therefore, if cost is the dominant consideration, GLuGAG has the potential to be a good choice, while still offering high performance. LFS-3 performance appears to be very similar to LSO, and may also be a good alternative if available at a lower cost. The rare-earth halides $LaBr_3$ and $CeBr_3$ offer good timing resolution (due to short decay time) and energy resolution (due to high light output), but due to their low density and Z_{eff}, their stopping power and hence sensitivity are low compared to LuAP, LSO and LFS-3. Their scatter fraction is also higher owing to the fact that the fraction of incident 511 keV photons which interact via photoelectric absorption rather than via Compton scattering will be higher in materials with higher Z_{eff}. Since they are hygroscopic, rare-earth halides also require encapsulation to avoid damage due to moisture.

4.1. Considerations for time of flight PET systems

The time-domain characteristics of the chosen scintillation material significantly impact the noise variance in the reconstructed image in time-of-flight (ToF) PET systems. To properly evaluate the timing performance of scintillation detectors for ToF PET systems using Monte Carlo simulations, it is necessary to accurately model the physics of the scintillation crystal geometry, scintillator surface finish, rise and decay time, photoelectron yield, single-electron response, transit time spread for the photodetector, amplifier impulse response, and the time pick-off method, all of which affect the scintillation detector timing resolution.

The expected simulated ToF spectra obtained from an ideal point source (zero positron range) located at the center of the scanner is exactly zero, while for a ^{18}F source, the spread would be of the order of 4.7 ps FWHM. In order to reproduce the reported ToF resolution of the Biograph mCT scanner (550 ps), additional jitter has to be included to spread the simulated arrival time in each detector using a different Gaussian blurring function for each scintillation material based on the scintillation materials properties. This is a major undertaking; in particular, characterising the time-domain behaviour of the scintillator to this level of detail will require full optical photon tracking to be enabled in the GATE scintillator model (although it would not require simulation of the full PET system). The quesion of optimal scintillator materials for ToF PET is both complex and interesting, and will be addressed in a future paper.

4.2. Simulation performance

Simulation throughput on a cluster of Intel Xeon CPUs (E5-2687W v2 3.40GHz) was approximately 2000 decays/sec/core; the simulation of 20 min-

utes of acquisition time on 20 cores with an initial activity of 40 MBq took around two weeks to complete. On more modern CPUs, the simulation time may be significantly reduced; simulation throughput scales near-linearly with the number of cores for this workload.

5. Conclusions

The validation study of the GATE model of the Siemens Biograph mCT PET/CT scanner showed very good agreement between simulated results and experimental measurements for a number of performance parameters, including scatter fraction, sensitivity, noise equivalent count rate and spatial resolution, characterised according to the specification of the NEMA NU 2-2007 standard. The performance of the simulated scanner was then evaluated with a range of different candidate scintillation materials having potential application in high performance PET scanners. The best performing materials were LuAP, LSO and LFS-3, which provided the highest sensitivity, lower scatter fraction and higher NECR for the same crystal depth. In contrast, rare-earth halides provide higher light yield, but much lower stopping power and hence sensitivity. With consideration of manufacturing costs, transparent rare earth ceramic garnet GluGAG provides a high light yield (nearly double that of LSO:Ce) and mid-range performance at a significantly lower cost compared to monocrystalline scintillators such as, LSO and LuAP. Therefore, this crystal provides a good compromise between cost and performance.

Acknowledgments

References

[1] Zaidi, H. (1999) Relevance of accurate Monte Carlo modeling in nuclear medical imaging. *Med Phys,* **26**(4), 574–608.

[2] Jan, S., Santin, G., Strul, D., Staelens, S., Assie, K., et al. (2004) GATE: a simulation toolkit for PET and SPECT. *Phys Med Biol,* **49**(19), 4543.

[3] Agostinelli, S., Allison, J., Amako, K., Apostolakis, J., Araujo, H., et al. (2003) Geant4 - a simulation toolkit. *Nucl Instrum Meth A,* **506**(3), 250–303.

[4] Allison, J., Amako, K., Apostolakis, J., Araujo, H., et al. (2006) Geant4 developments and applications. *IEEE T Nucl Sci,* **53**(1), 270–278.

[5] Jan, S., Benoit, D., Becheva, E., Carlier, T., et al. (2011) GATE V6: a major enhancement of the GATE simulation platform enabling modelling of CT and radiotherapy. *Phys Med Biol,* **56**(4), 881.

[6] Schmidtlein, C. R., Kirov, A. S., Nehmeh, S. A., Erdi, Y. E., et al. (2006) Validation of GATE Monte Carlo simulations of the GE Advance/Discovery LS PET scanners. *Med Phys,* **33**(1), 198–208.

[7] Gonias, P., Bertsekas, N., Karakatsanis, N., Saatsakis, G., et al. (2007) Validation of a GATE model for the simulation of the Siemens biograph^{TM}6 PET scanner. *Nucl Instrum Meth A,* **571**(1), 263–266.

[8] Lamare, F., Turzo, A., Bizais, Y., Le Rest, C. C., and Visvikis, D. (2006) Validation of a Monte Carlo simulation of the Philips Allegro/GEMINI PET systems using GATE. *Phys Med Biol,* **51**(4), 943.

[9] Poon, J. K., Dahlbom, M. L., Casey, M. E., Qi, J., Cherry, S. R., and Badawi, R. D. (2015) Validation of the SimSET simulation package for modeling the Siemens Biograph mCT PET scanner. *Phys Med Biol,* **60**(3), N35.

[10] Abushab, K. M., Herraiz, J. L., Vicente, E., Cal-Gonzlez, J., Espaa, S., et al. (2016) Evaluation of PeneloPET Simulations of Biograph PET/CT Scanners. *IEEE T Nucl Sci,* **63**(3), 1367–1374.

[11] Surti, S. and Karp, J. (2005) A count-rate model for PET scanners using pixelated Anger-logic detectors with different scintillators. *Phys Med Biol,* **50**(23), 5697.

[12] Michel, C., Eriksson, L., Rothfuss, H., Bendriem, B., Lazaro, D., and Buvat, I. (2006) Influence of crystal material on the performance of the HiRez 3D PET scanner: A Monte-Carlo study. In *Nucl Sci Symp Conf Rec* Vol. 4, pp. 2528–2531.

[13] Eriksson, L., Townsend, D., Eriksson, M., Melcher, C., , et al. (2004) Experience with scintillators for PET: towards the fifth generation of {PET} scanners. *Nucl Instrum Meth A,* **525**(1-2), 242 – 248.

[14] Perkins, A., Stearns, C., Chapman, J., Kolthammer, J., et al. (2007) NEMA Standards Publication NU 2-2007: Performance measurements of positron emission tomographs. *Rosslyn USA: National Electrical Manufacturers Association (NEMA),*.

[15] Yang, X. and Peng, H. (2015) The use of noise equivalent count rate and the NEMA phantom for PET image quality evaluation. *Phys Medica,* **31**(2), 179–184.

[16] Wagatsuma, K., Miwa, K., Sakata, M., Oda, K., Ono, H., Kameyama, M., Toyohara, J., and Ishii, K. (2017) Comparison between new-generation SiPM-based and conventional PMT-based TOF-PET/CT. *Phys Medica,* **42**, 203–210.

[17] Jakoby, B., Bercier, Y., Conti, M., Casey, M., et al. (2011) Physical and clinical performance of the mCT time-of-flight PET/CT scanner. *Phys Med Biol,* **56**(8), 2375.

[18] Brun, R. and Rademakers, F. (1997) ROOT - An object oriented data analysis framework. *Nucl Instrum Meth A,* **389**(1), 81–86.

[19] Loening, A. M. and Gambhir, S. S. (2003) AMIDE: a free software tool for multimodality medical image analysis. *Mol Imag,* **2**(3), 131–137.

[20] Thielemans, K., Tsoumpas, C., Mustafovic, S., Beisel, T., et al. (2012) STIR: software for tomographic image reconstruction release 2. *Phys Med Biol,* **57**(4), 867.

[21] Melcher, C., Schweitzer, J., Utsu, T., and Akiyama, S. (1990) Scintillation properties of GSO. *IEEE T Nucl Sci,* **37**(2), 161–164.

[22] Chewpraditkul, W., Swiderski, L., Moszynski, M., Szczesniak, T., et al. (2009) Scintillation properties of LuAG: Ce, YAG: Ce and LYSO: Ce crystals for gamma-ray detection. *IEEE T Nucl Sci,* **56**(6), 3800–3805.

[23] Van Loef, E., Dorenbos, P., Van Eijk, C., Krämer, K., and Güdel, H. (2002) Scintillation properties of LaBr 3: Ce 3+ crystals: fast, efficient and high-energy-resolution scintillators. *Nucl Instrum Meth A,* **486**(1), 254–258.

[24] Van Eijk, C. W. et al. (2002) Inorganic scintillators in medical imaging. *Phys Med Biol,* **47**(8), R85–R106.

[25] Moszynski, M., Kapusta, M., Wolski, D., Szawlowski, M., and Klamra, W. (Jun, 1998) Energy resolution of scintillation detectors readout with large area avalanche photodiodes and photomultipliers. *IEEE T Nucl Sci,* **45**(3), 472–477.

[26] Moses, W. W. (2002) Current trends in scintillator detectors and materials. *Nucl Instrum Meth A,* **487**(1-2), 123 – 128.

[27] Iltis, A., Mayhugh, M., Menge, P., Rozsa, C., et al. (2006) Lanthanum halide scintillators: Properties and applications. *Nucl Instrum Meth A,* **563**(2), 359–363.

[28] Cherepy, N. J., Payne, S. A., Asztalos, S. J., Hull, G., et al. (2009) Scintillators with potential to supersede lanthanum bromide. *IEEE T Nucl Sci,* **56**(3), 873–880.

[29] van Loef, E., Dorenbos, P., van Eijk, C., Krmer, K., and Gdel, H. (2002) Scintillation properties of LaBr3:Ce3+ crystals: fast, efficient and high-energy-resolution scintillators. *Nucl Instrum Meth A,* **486**(1-2), 254 – 258.

[30] Shah, K. S., Glodo, J., Higgins, W., van Loef, E. V., et al. (2004) CeBr$_3$ scintillators for gamma-ray spectroscopy. In *Nucl Sci Symp Conf Rec* IEEE Vol. 7, pp. 4278–4281.

[31] Quarati, F., Dorenbos, P., Van der Biezen, J., Owens, A., et al. (2013) Scintillation and detection characteristics of high-sensitivity CeBr$_3$ gamma-ray spectrometers. *Nucl Instrum Meth A,* **729**, 596–604.

[32] Szupryczynski, P., Spurrier, M. A., Rawn, C. J., Melcher, C. L., et al. (2005) Scintillation and optical properties of LuAP and LuYAP crystals. In *Nucl Sci Symp Conf Rec* Vol. 3, pp. 1305–1309.

[33] Moszyński, M., Wolski, D., Ludziejewski, T., Kapusta, M., Lempicki, A., et al. (1997) Properties of the new LuAP: Ce scintillator. *Nucl Instrum Meth A,* **385**(1), 123–131.

[34] Del Guerra, A. (2004) Ionizing Radiation Detectors for Medical Imaging, World Scientific Pub Co Inc, .

[35] Kuwano, Y., Saito, S., and Hase, U. (1988) Crystal growth and optical properties of Nd: GGAG. *J Cryst Growth,* **92**(1), 17–22.

[36] David, S., Georgiou, M., Fysikopoulos, E., and Loudos, G. (2015) Evaluation of a SiPM array coupled to a Gd3Al2Ga3O12:Ce (GAGG:Ce) discrete scintillator. *Phys Medica,* **31**(7), 763–766.

[37] Surti, S. and Karp, J. S. (2016) Advances in time-of-flight PET. *Phys Medica,* **32**(1), 12–22.

[38] Wu, Y., Luo, Z., Jiang, H., et al. (2015) Single crystal and optical ceramic multicomponent garnet scintillators: A comparative study. *Nucl Instrum Meth A,* **780**, 45–50.

[39] Grodzicka, M., Moszyński, M., Szczkeśniak, T., Syntfeld-Każuch, A., et al. (2011) Characterization of LFS-3 scintillator in comparison with LSO. *Nucl Instrum Meth A,* **652**(1), 226–230.

[40] David, S., Michail, C., Valais, I., et al. (2015) Investigation of luminescence properties of Lutetium Fine Silicate (LFS-3) scintillation crystals under X-ray radiographic conditions. In *Proc 2015 SCinTE* p. 71.

[41] Poon, J. K., Dahlbom, M. L., Moses, W. W., Balakrishnan, K., Wang, W., Cherry, S. R., and Badawi, R. D. (2012) Optimal whole-body PET scanner configurations for different volumes of LSO scintillator: a simulation study. *Phys Med Biol,* **57**(13), 4077.

List of Tables

Table 1: Siemens Biograph mCT PET scanner design parameters, as used in the GATE simulations.

Parameter	Value
Number of block rings	4
Detector blocks per ring	48
Scintillator material	LSO
Crystals per block	13×13 = 169
Crystals per axial ring	624
Axial FOV	218 mm
Transaxial FOV	700 mm
Number of image planes	109
Coincidence time window	4.1 ns
Energy window	435-650 keV
Energy resolution	11.7%
Crystal pitch	4 mm
Crystal length (thickness)	20 mm
Detector ring diameter	842 mm
Time resolution	527.5 ps
Maximum ring difference	49
Number of crystals in one module	13×13=169
Number of crystals in one sector	169×4=676
Number of crystals	676×48=32448 crystals

Table 2: Specific properties of candidate inorganic scintillator materials used in this simulation. Decay time refers to the dominant decay component.

Scintillator	Light yield (ph/MeV)	Decay time (ns)	Density (g/cm^3)	Effective atomic no.	Energy resol. @511 keV (%)	Hygroscopic	Refs.
LaBr$_3$:Ce	63000	16	5.29	44.1	2.6	yes, highly	[23, 27, 29]
CeBr$_3$	68000	17	5.2	45.9	3.6	yes, highly	[30, 31]
LSO	25000	40	7.4	65	8.4	no	[21, 26, 22]
LuAP	11400	16.5	8.34	65	9	no	[32, 33]
LFS-3	30000	33	7.34	64	8	no	[39]
GLuGAG:Ce	60000	40	6.7	55.2	7.1	no	[37, 38]

Table 3: Comparison of spatial resolution results obtained from GATE simulations of the Siemens Biograph mCT PET scanner with published values obtained via simulation and experimental measurement. R_{CFoV} is the radial distance from the centre of the field of view. The dimensions are in mm.

Parameter	R_{CFoV}	Experimental [17]		GATE (this work)		SimSet [9]		PeneloPET [10]	
	(mm)	FWHM	FWTM	FWHM	FWTM	FWHM	FWTM	FWHM	FWTM
Transverse	10	4.4±0.1	8.6±0.1	3.8	7.8	3.3	7.4	4.6	8.5
Axial	10	4.4±0.1	8.7±0.2	3.4	7.6	3.1	7.0	4.2	4.5
Transverse radial	100	5.2±0.0	9.4±0.1	4.6	8.6	4.3	8.2	5.5	9.0
Transverse tangential	100	4.7±0.1	9.2±0.1	4.0	8.0	3.8	7.6	5.6	10.2
Axial	100	5.9±0.0	10.9±0.3	5.5	10.2	5.3	9.7	4.4	7.5

Table 4: Sensitivity measurements (in kcps.MBq^{-1}) at two different locations within the Siemens Biograph mCT PET scanner, and scatter fraction and noise equivalent count rate.

Parameter	Location	Experimental [17]	GATE (this work)	SimSet [9]	PeneloPET [10]
Sensitivity	(0, 0, 0)	9.7±0.2	9.65	–	9.8
	(0, 100, 0)	9.5±0.1	9.48	–	9.8
Scatter Fraction (%)	(0, -45, 0)	33.2	34.35	38.48	34.8
NECR (kcps@kBq.mL^{-1})	(0, -45, 0)	180.3@29	188@25	180@24	177@34

Table 5: Performance characteristics for the mCT PET scanner for each of the evaluated scintillation materials. Locations are in mm.

Parameter	Location	Experimental [17]	LSO	CeBr$_3$	LFS-3	GluGAG	LuAP	LaBr$_3$
Sensitivity (kcps.MBq^{-1})	(0,0,0)	9.7±0.2	9.65	2.22	9.52	6.86	10.53	2.02
	(0,100,0)	9.5±0.1	9.48	2.25	9.46	6.80	10.39	1.98
Scatter fraction (%)	(0,-45,0)	33.2	34.35	36.32	34.54	35.22	34.42	36.39
NECR (kcps@kBq.mL^{-1})	(0,-45,0)	180.3 @29	188 @25	54.21 @20	186.82 @25	139.72 @25	198.43 @20	39.27 @20

List of Figures

Figure 1: Graphical representation of the GATE modelled Siemens Biograph mCT PET scanner with NEMA cylindrical scatter phantom in the field of view.
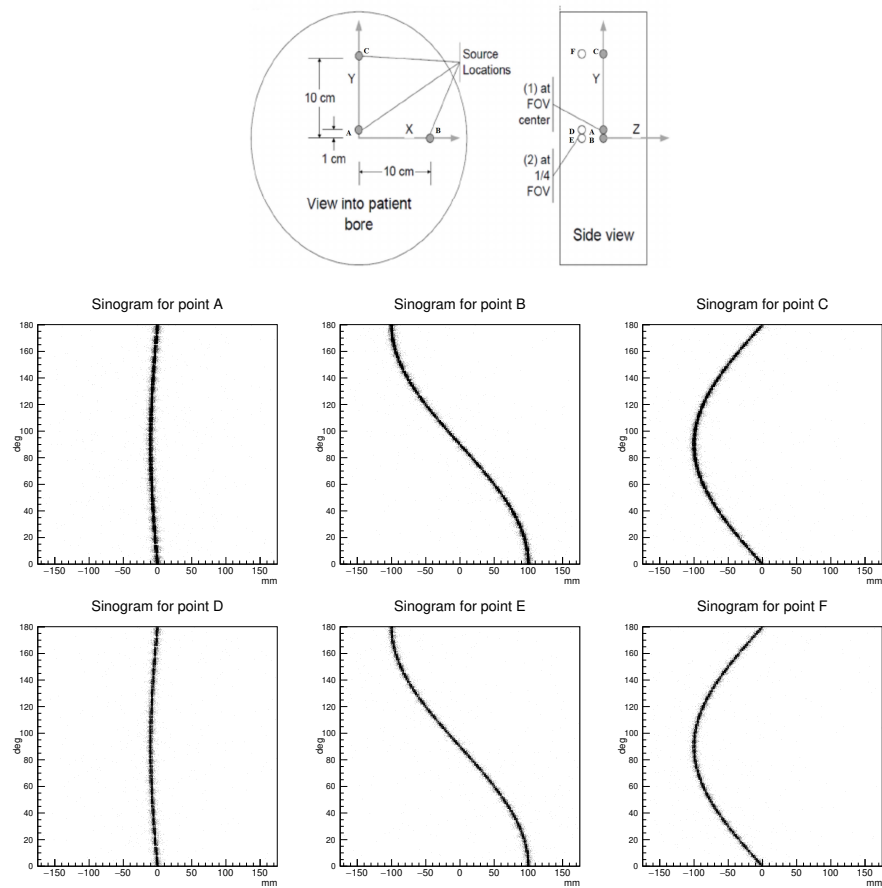
Figure 2: The NEMA NU 2-2007 spatial resultion result sinograms for the GATE simulation model of the Siemens Biograph mCT scanner for six different transaxial and axial positions.

23
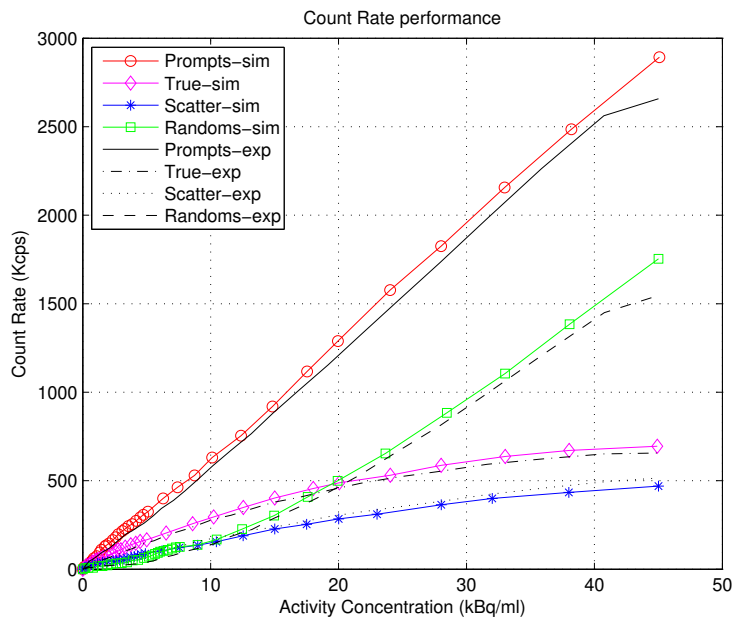
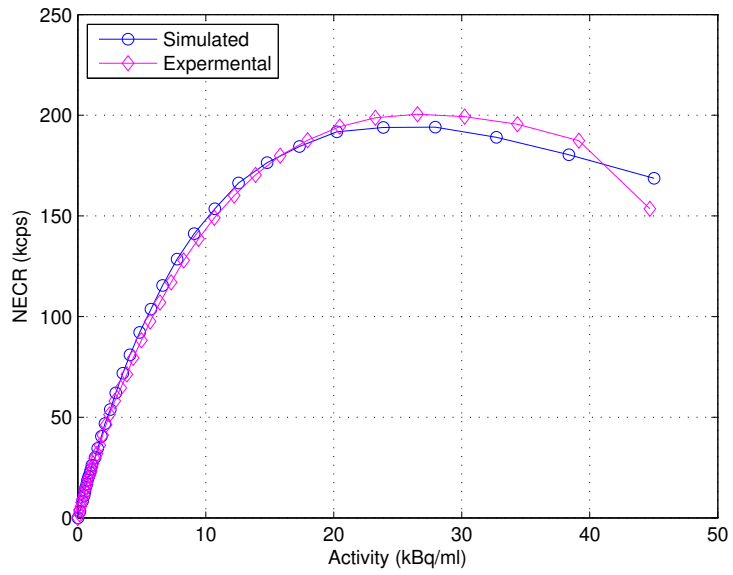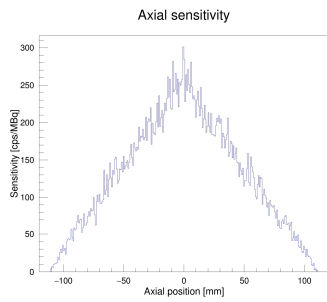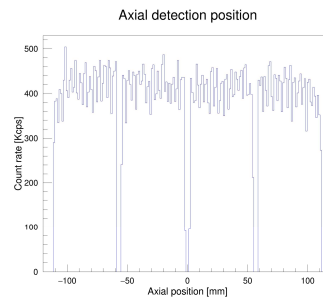Figure 3: Count rate performance for the simulated mCT PET scanner(symbols), compared to experimental results published in [17].
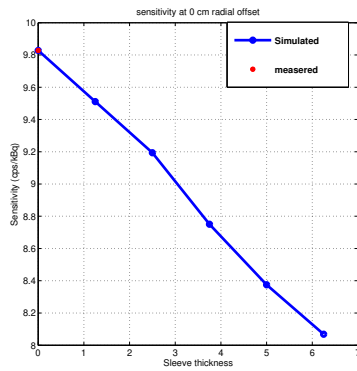
Figure 4: NECR performance for the simulated mCT PET scanner, compared to experimental data published in [17].
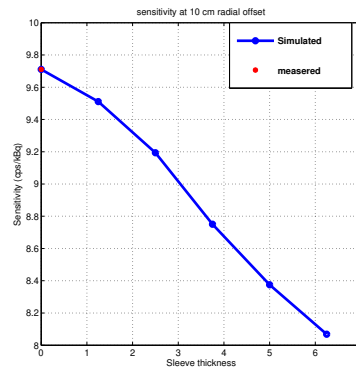
(a)

(b)

(c)

(d)

Figure 5: Sensitivity performance for the simulated mCT PET scanner. Where (a) is the axial sensitivity, (b) is the axial detection position, (c) is the sensitivity at the center of the field-of-view, and (d) is the sensitivity at 10 cm radial offset.
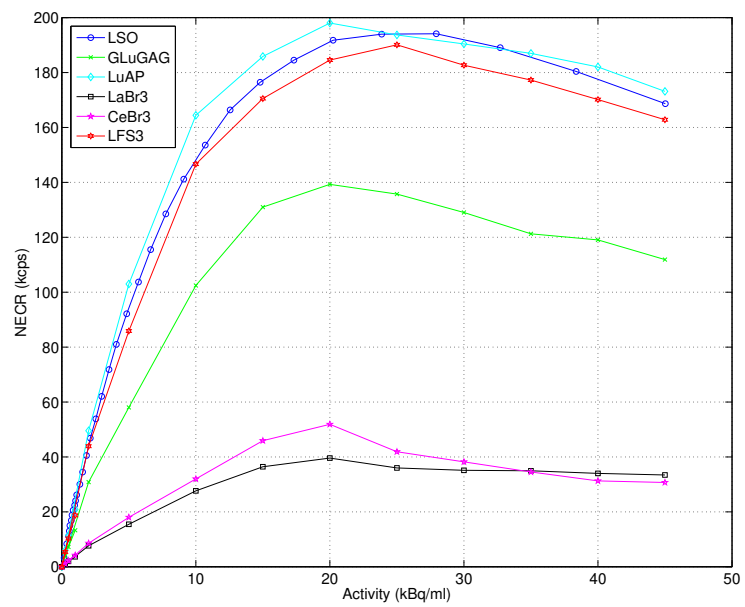
26

Figure 6: NECR of the mCT PET scanner vs. activity concentration for each of the evaluated scintillation materials.